CHITOSAN NANOBUBBLES DEVELOPMENT AND EVALUATION FOR THE DELIVERY OF SUNITINIB-AN ANTICANCER AGENT

KISHORE KUMAR M., JAYA PRAKASH D., BASAVA RAO V. V.

¹University College of Technology, Osmania University, Hyderabad, Telangana 500007, India
Email: kishorerati14@gmail.com

ABSTRACT

Objective: In the current study, we introduced a novel method for creating Sunitinib nanobubbles by incorporating it into chitosan-shelled nanobubbles.

Methods: The Design Expert® programme randomly assigned around 13 experiments, and multiple regression analysis was used to statistically examine the data. The effect of the amount of sunitinib, amount of chitosan, amount of Epikuron 200, amount of palmitic acid and stirring speed, on percent encapsulation efficiency and drug load while maintain minimum particle size of nanobubbles as considered through a definitive screening plan. By placing limitations on the response parameters, the optimum formulation was created using a numerical optimization approach. The three improved formulations (Batch1 through Batch3) were assessed.

Results: The findings show that the nanobubbles particle size of 78.56-82.42 nm with an encapsulation efficiency of 68.48-69.56 % and loading capacity of 23.88-25.02%. The quantity of sunitinib released from nanobubbles was much larger (96.52 percent) than that from the sunitinib solution within 24 h, according to an *in vitro* release profile of the medication using ultrasonography. The hemolytic activity of the blank nanobubbles and sunitinib-loaded nanobubbles was measured to assess their safety up to a concentration of 10 mg/ml. With erythrocytes, drug-loaded nanobubbles had a good safety profile. FTIR, DSC studies indicated no chemical interactions, TEM images revealed nanobubbles size of 70-100 nm and stability studies shows no significant changes.

Conclusion: For contrast-enhanced tumour imaging and subsequent therapeutic administration, nanobubbles were found to be superior.

Keywords: Sunitinib, Anti-tumor agent, Chitosan shelled nanobubbles, Perfluoropentane, Definitive screening design (DSD)

INTRODUCTION

Sunitinib antidepressant drug is associate in nursing oral oxindol, a multitargeted aminoalkanoic acid enzyme substance that has potent anti-angiogenic effects and direct growth activities [1]. Sunitinib is given orally, once daily as a 50-mg capsule over four weeks, followed by a 2-week rest period, in perennial 6-week treatment cycles. Sunitinib is primarily metabolized by CYP 3A4 to its active N-desethyl metabolite and is subject to presystemic metabolism by this enzyme. Because of the long terminal half-life of sunitinib (40-60 h), steady-state concentration is not achieved until 2 w of continuously daily dosing [2]. At this dose, numerous adverse effects have been observed. For this reason, effective and safe sunitinib delivery systems are urgently required so that direct delivery of sunitinib into the respiratory organ might increase the native concentration of the drug, whereas minimizing its concentration within the remainder of the body. Some drug carrier systems such as microspheres, polymeric nanoparticles, self-nano emulsifying drug delivery systems, Micellar Nanocomplex, copper complex have stayed studied in literature to enhance *in vitro* dissolution speed and therapeutic efficacy of sunitinib in literature [3-5].

Amongst the various drug delivery systems, Due to the intrinsic differences between an anticancer environment and a healthy environment, smart systems have become crucial to the administration of anticancer drugs. A smart medication delivery system may react to sudden environmental stimuli, such as chemical ones. To acquire triggered medication delivery, pressure waves and ultrasonic (US) have been extensively examined as external stimulus [6].

In order to optimise the stability and bio-distribution of the delivered medicine to the diseased location, nanobubbles are spherical core/shell structures filled with gases or vaporizable chemicals, such as perfluorocarbons, and have diameters in the nanometer order of magnitude. Nanobubbles have shown promising results as novel nanocarriers with improved stability and high drug-loading capacity, and extravasation capability. Both the Enhanced Permeability and Retention effect and active targeting, or antibodies attaching to the bubble surface, may cause them to collect within tumour tissues [7, 8].

Chitosan is more advantageous as a carrier for anticancer medications since it has both direct and indirect antitumor effects [9]. In this study, we intended towards progress chitosan nanobubbles containing sunitinib with the right size and physicochemical qualities to enhance the therapeutic efficacy of the drug using definitive screening since chitosan has both direct and indirect antitumor effects, it is more favorable as a carrier for anticancer drugs [10].

MATERIALS AND METHODS

Chitosan as well as additional excipients, were purchased at Sigma-Aldrich in place India, while Sunitinib was indeed presented from Dr. Reddy's Lab in Hyderabad, India. Purchase of perfluoropentane from Pharm Affiliates in Haryana, India.

Chitosan-shelled nanobubble preparation

Perfluoropentane was used to create the inner core of the nanobubbles, and medium molecular weight chitosan, with a deacetylation level of 75–85 percent (approximately 190,000 Da) was used to create the outside shell.

With a little modification, nanobubbles were created using the approach described earlier [11, 12]. Preparation of sunitinib loaded chitosan nanobubbles

Accurately weighed quantity of sunitinib was dissolved in perfluoropentane core using ethanol as co-solvent to facilitate drug dissolution. Sunitinib-perfluoropentane solution was mixed with ethanol-dissolved epikuron 200 and palmitic acid to create a prior emulsion. The process was comparable to that applied to chitosan-coated nanobubbles.

Design about the experiments

To examine the influence of five continuous parameters, the DSD was used. (k = 5) that as the amount of sunitinib, amount of chitosan, amount of Epikuron 200, amount of palmitic acid and stirring speed. Finding a combination of the five elements that maximises the % is the aim of the experiment encapsulation efficiency and drug load while maintain minimum particle size (table 1).

Table 1: Definitive screening design and experimental data of responses

Run	Factor 1	Factor 2	Factor 3	Factor 4	Factor 5	Response 1	Response 2	Response 3
	A: Amount of sunitinib	B: Amount of chitosan	C: Amount of epikuron 200	D: Amount of palmitic acid	E: Stirring speed	Encapsulation efficiency	Drug loading	Particle size
	mg	% w/v	% w/v	% w/v	rpm	%	%	nm
1	350	4	2	1	14000	63.62	28.26	145.34
2	200	4	1.5	1	8000	70.28	18.73	226.48
3	200	2	1	1	11000	65.12	16.34	184.56
4	500	4	1	0.6	8000	63.42	24.56	322.34
5	200	3	2	0.2	8000	63.88	14.48	358.92
6	200	4	1	0.2	14000	71.28	20.12	138.36
7	500	2	2	1	8000	51.32	22.34	384.54
8	500	4	2	0.2	11000	59.42	26.34	339.82
9	500	3	1	1	14000	59.86	28.82	162.56
10	350	3	1.5	0.6	11000	61.24	21.88	262.48
11	350	2	1	0.2	8000	59.22	14.26	372.86
12	200	2	2	0.6	14000	60.87	19.26	212.66
13	500	2	1.5	0.2	14000	54.42	23.92	306.58

Data analysis

After the design has been made, its characteristics may be researched. The whole second-order model has the following structure for 5 factors:

$$Y = \beta_0 + \beta_1 X_1 + \beta_2 X_2 + \beta_3 X_3 + \beta_4 X_4 + \beta_5 X_5 + \beta_{1,2} X_1 X_2 + \beta_{1,3} X_1 X_3 + \beta_{1,4} X_1 X_4$$
$$+ \beta_{1,5} X_1 X_5 + \beta_{2,3} X_2 X_3 + \beta_{2,4} X_2 X_4 + \beta_{2,5} X_2 X_5 + \beta_{3,4} X_3 X_4 + \beta_{3,5} X_3 X_5$$
$$+ \beta_{4,5} X_4 X_5 + \beta_{1,1} X_1^2 + \beta_{2,2} X_2^2 + \beta_{3,3} X_3^2 + \beta_{4,4} X_4^2 + \beta_{5,5} X_5^2$$

Somewhere, Y–Retort parameter

β_0–Intercept-constant term

β_1–β_5–Regression coefficients

β_{12}, β_{13}, $\beta_{14,}$ β_{23} β_{24} and β_{34}–Interface coefficients

β_{11}, β_{22}, β_{33}, β_{44} and β_{55}–Quadratic coefficients

X_1, X_2, X_3, X_4 and X_5–Main influencing factors

$X_1 X_2$–two-factor Interactive effect

X_1^2, X_2^2, X_3^2, X_4^2 and X_4^2–Quadratic terms

Optimization

By placing constraints using numerical optimization, the optimal locations for the independent variables were found on the response parameters and influencing factors approach. Under ideal circumstances, the nanoformulation was created in three copies to confirm the efficacy of the optimization method.

Formulation of nanobubbles and their characterization

Determination of particle size, zeta potential and polydispersity index

The normal particle extent and polydispersity index remained resolute by measuring the usage of a Malvern particle size analyzer to measure the sporadic variation in light intensity radiated by nanoliposomal dispersion (Master sizer 2000). The zeta potential at a count frequency at 250 particles/second and 25 °C of nanobubbles was determined in a U-shaped cell with an extra gold-plated electrode. Three times' worth of measurements were taken in total.

Loading capacity and encapsulation efficiency

Encapsulation efficacy of nanobubbles is premeditated by determining both bound and unbound drug in the system [13]. The percentage encapsulation effectiveness and loading capacity stayed likely as per the subsequent calculations:

Encapsulation efficiency
$$= \frac{(\text{Total amount of Sunitinib} - \text{Free Sunitinib})}{\text{Total amount of Sunitinib}}$$

$$\text{Loading capacity} = \frac{(\text{Total amount of Sunitinib} - \text{Free Sunitinib})}{\text{Weight of nanobubbles formulation}}$$

Drug release *in vitro* in the presence and absence of ultrasound

Sunitinib's *in vitro* release kinetics from the nanobubbles were assessed using the dialysis bag technique at 37 °C in both the presence and absence of ultrasound. Sunitinib nanobubbles aqueous suspension (equivalent to 50 mg of sunitinib) were placed in a dialysis bag (Spectrapore cellulose dialysis membrane, cut off = 12–14 kDa) and utilised as the donor phase in a 120 ml phosphate buffer (0.01 M, pH 7.4). (Receiving phase). Sunitinib Withdrawing 1 ml of the receiving phase at a set time and replacing it with 1 ml of fresh phosphate buffer allowed the release time to be calculated up to 24 h. The release was also seen following the application of ultrasound (with a frequency of 2.5 0.1 MHz and an insonation period of one minute). The medication release remained monitored intended for 24 h afterward the insonation of nanobubbles in the dialysis bag, as previously mentioned. To determine the drug concentration, spectrophotometric analysis was performed on all the removed samples [14].

Fourier transform infrared (FTIR)

To verify the identification of the drug and excipients and to discover how the drug interacted with the excipients, FTIR absorption spectra of the pure drug, all the chosen excipients utilised, and the physical combination of the drug and excipients were collected.

Differential scanning calorimetry

Thermal analysis of sunitinib, Chitosan, Epikuron 200, palmitic acid, blank nanobubbles and sunitinib-loaded nanobubbles was performed using Shimadzu DS 60 Thermal Analyzer. For every sample, three runs were made.

Transmission electron microscopy (TEM)

The form and size of nanobubbles were examined using an HF5000 transmission electron microscope.

Calculation of haemolytic activity

In human blood, the chitosan nanobubbles' hemolytic activity was assessed. According to the procedure reported elsewhere [15]. The percent hemolysis was calculated using the following equation.

$$\% \text{ Hemolysis} = \frac{ABS_{Sample} - ABS_0}{ABS_{100} - ABS_0} \times 100$$

Where ABS_0 and ABS_{100} are the absorbance of the solution at 0 and 100 % hemolysis, respectively.

Assessment of constancy of sunitinib nanobubbles

For 6 mo, sunitinib nanobubble stability was tested at four (4 °C, 25 °C, and 40 °C) are three distinct temperatures. On the first, the fifteenth, the ninetieth, and the eighty-first days, the sunitinib content, encapsulation effectiveness, and average particle size of sunitinib-loaded nanobubbles were assessed. In order to assess the structural integrity of sunitinib-loaded nanobubbles, optical microscopy was also used to study their appearance.

RESULTS AND DISCUSSION

Definitive screening design–model evaluation

The selected DSD a major model was discovered in terms of encapsulation efficacy, drug loading and particle size, as shown by the associated p values having a significance level of less than 0.05. The diagram depicting the design's outline may be seen in fig. 1 [16].

Fig. 1: Summary of the definitive screening design

Data fitting ad modelling

Thirteen trials were conducted in a set according to a five-factor, three-level DSD. Table 1 presents the findings after the randomised trials intended for the chosen autonomous factors as well as dependent variables. The encapsulation efficiency (R1) for all the trials was found to be in the range of 51.32–71.28 %. The drug loading ranges from 14.26-28.82 %. The particle size varied from 138.36-384.54 nm. Resultant data was analysed by means of Stat-Ease Design Expert ® (V13.0.9.0) software to find analysis of variance, regression coefficients and regression equation. All of the findings were fitted into a linear model, and the ANOVA and multiple regression coefficient (R2) values supported the model's suitability.

The response surface for each parameter was modelled using a general regression equation. The equation in terms of coded factors can be used to make predictions about the response for given levels of each factor. By default, the high levels of the factors are coded as+1 and the low levels are coded as-1. The coded equation is useful for identifying the relative impact of the factors by comparing the factor coefficients. The regression equations obtained following the response transformation are shown in table 2 for all the variables. it is easy to predict the factorial impact by looking at the coefficient. Multiple linear regression analysis for all the models is shown in terms of R^2 value, adjusted R^2 value, predicted R^2 value and coefficient of variation (table 2). The values of R^2 were high, implying the good performance of the proposed models. The values of Adjusted R^2 were in good agreement with predicted R^2, indicating the capability of the proposed models to predict the response for a new observation. The predicted R^2 values were not noticeably less than R^2, inferring that the model was not over fitting.

Fig. 2: Model summary statistics–encapsulation efficiency

Table 2: Regression equations for the responses–encapsulation efficiency, drug loading and particle size

Dependent variable	Regression equation	R^2	Adjusted R^2	Predicted R^2	CV
Encapsulation efficiency (R1)	61.84-4.30 A+3.71 B–1.98 C+0.19 D+0.19 E	0.9933	0.9885	0.9749	0.9546
Drug loading (R2)	21.49+3.71 A+2.19 B+0.65 C+1.54 D+2.60 E	0.9968	0.9945	0.9888	1.67
Particle size (R3)	262.88+39.49 A-28.89 B+26.06 C–41.31 D–69.96 E	0.9988	0.998	0.9956	1.53

Encapsulation efficiency

The encapsulation efficiency of sunitinib within chitosan nanobubbles was ranged from 51.32 to 71.28 % as presented in table 1. Statistical analysis of data suggested that the model can fit a linear model with focus on the model maximizing the Adjusted R^2 and the Predicted R^2. The model summary statistics remains by means of fig. 2 and the discrete effects of A, B, C, D and E on encapsulation efficiency were depicted in the individual effects plot and perturbation plot fig. 3 and 4.
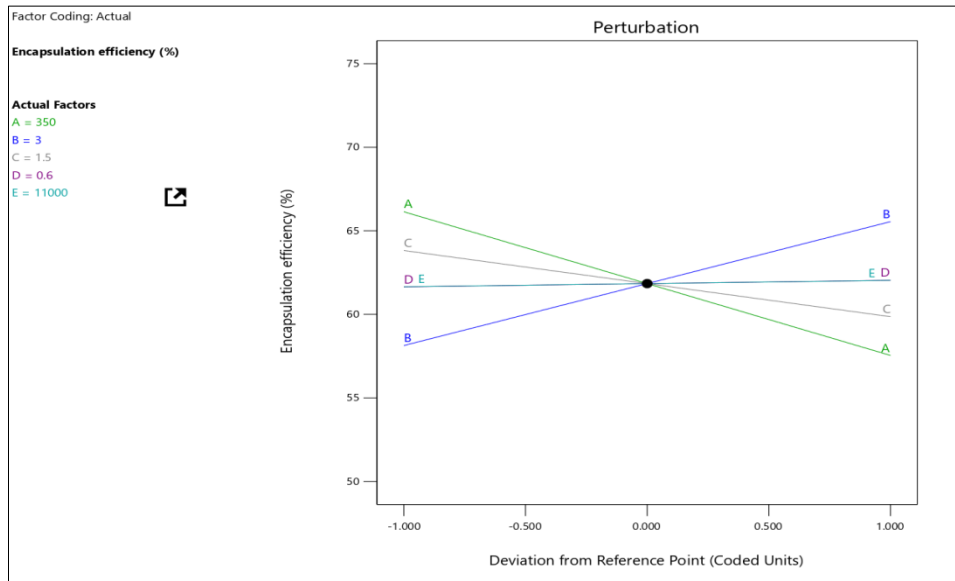
Fig. 3: Perturbation plot showing the effect of A, B, C, D and E on encapsulation efficiency
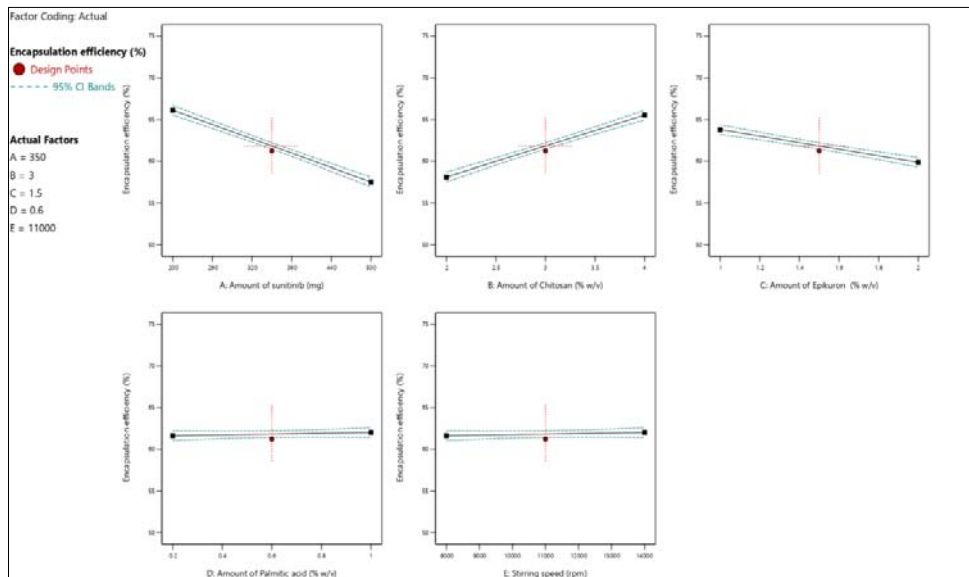
Fig. 4: Individual value plot showing the effect of A, B, C, D and E on encapsulation efficiency

Drug loading

The technique of incorporating a medicine into a polymer matrix or capsule is known as drug loading and 40 °C). The percent drug loading of sunitinib nanobubbles was ranged from 14.26 to 28.82 % as presented in table 1. Statistical analysis of data suggested that the model can fit a linear model with focus on the model maximizing the Adjusted R^2 and the Predicted R^2.

The model summary statistics as displayed in fig. 5. The individual effects like A, B, C, D and E on drug loading were depicted in the individual effects plot and perturbation plot (fig. 6 and 7).
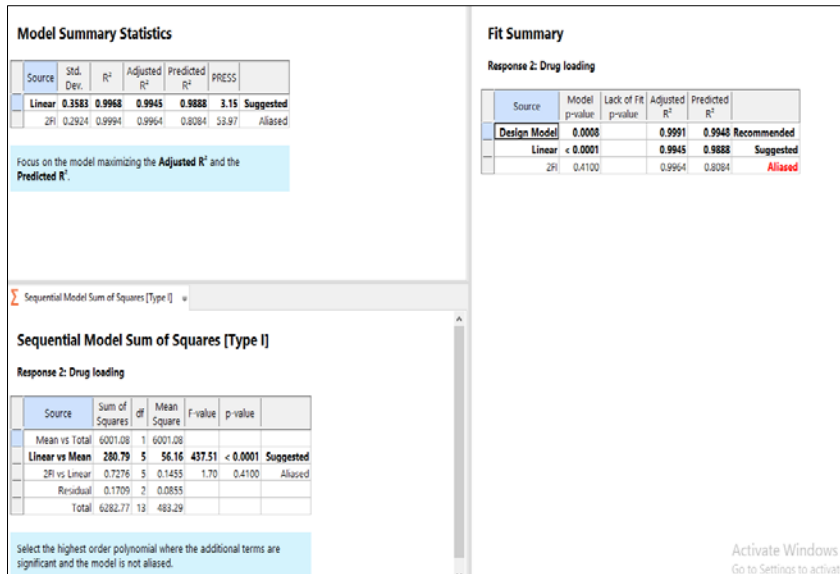
Fig. 5: Model summary statistics–drug loading
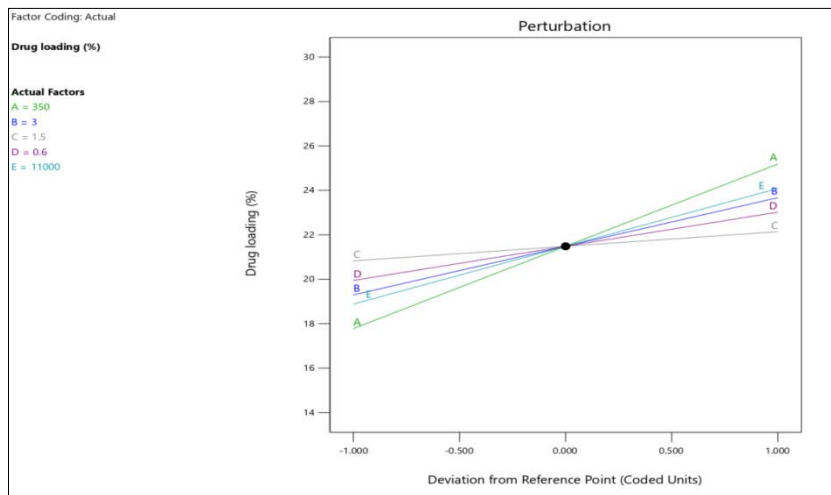
Fig. 6: Perturbation plot showing the effect of A, B, C, D and E on percent drug loading
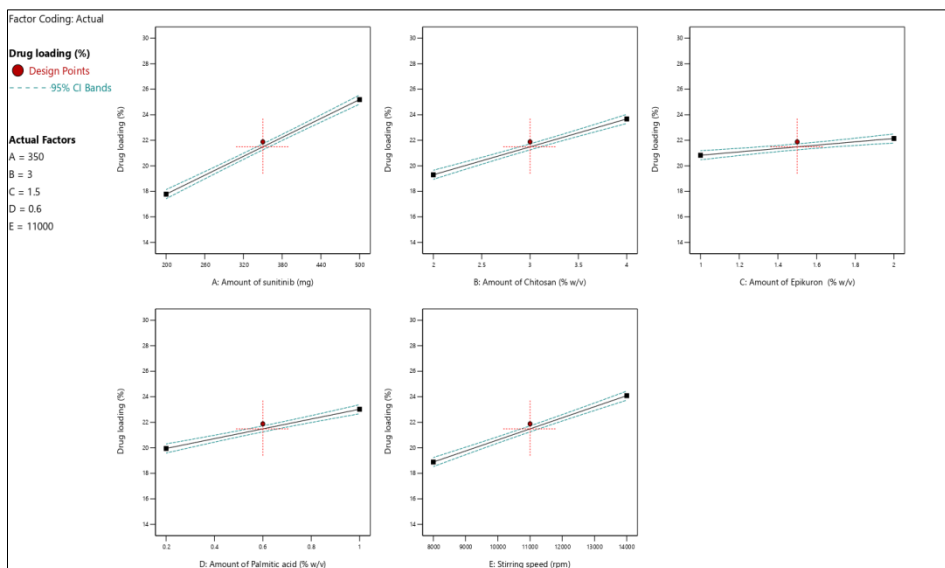
Fig. 7: Individual value plot showing the effect of A, B, C, D and E on percent drug loading

Particle magnitude

The range of the nanobubbles' particle sizes was discovered to be 138.36-384.54 nm as presented in table 1. Statistical analysis of data suggested that the model can fit a linear model with focus on the model maximizing the Adjusted R^2 and the Predicted R^2. The model summary statistics is as shown in fig. 8 [17]. The individual effects of A, C, D, B and E on particle magnitude were depicted in the individual effects plot and perturbation plot (fig. 9 and 10).
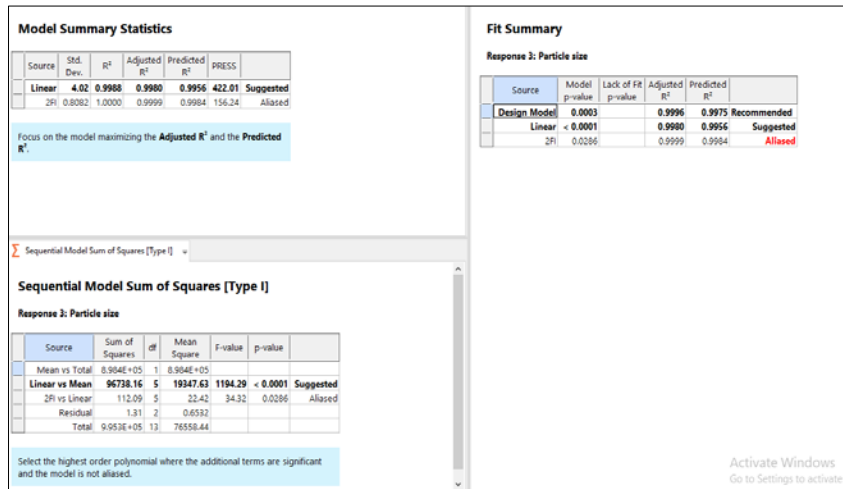
Fig. 8: Model summary statistics–particle size
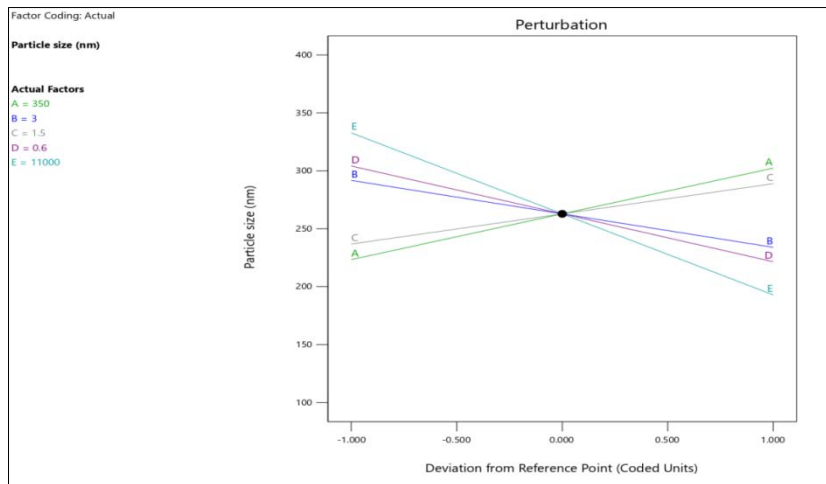
Fig. 9: Perturbation plot showing the effect of A, B, C, D and E on particle size
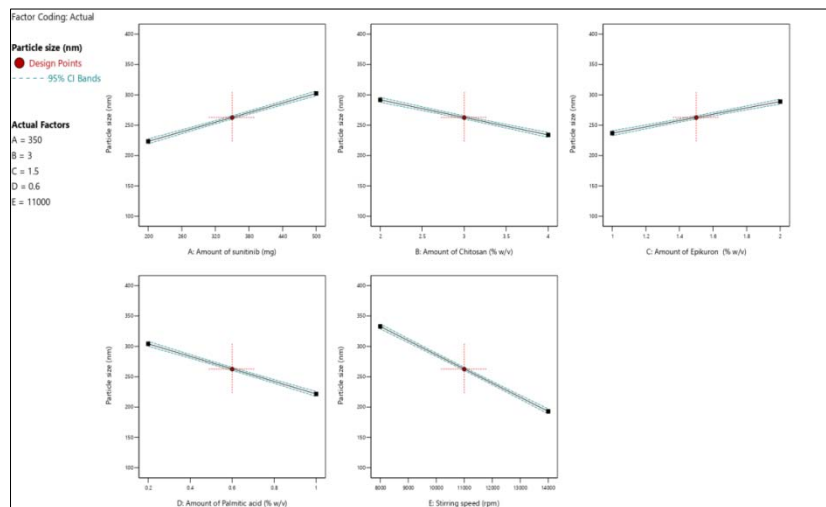
Fig. 10: Individual value plot showing the effect of A, B, C, D and E on particle size

Response optimization

When a large number of responses are required to be optimized, the desirability function is the most popular mathematical tool to be employed. The desirability function is a mathematical method to analyze a multi-response optimization problem. The desirability function is based on an idea that a product or process can contain the simultaneous study of several quality characteristics and it may be totally unacceptable for the customer if one of them is missing. Its goal is to find working conditions to ensure compliance with all the relevant standards in response and, at the same time, to provide the optimum compromise in the desirable joint response. Derringer function static (D) is calculated using the following equation.

$$D = (d_1(\hat{y_i}) \times d_2(\hat{y_2}) \times \cdots \times d_m(\hat{y_m}))^{1/m} = \left(\prod_{i=1}^{m} d_i(\hat{y_i})\right)^{1/m}$$

All three responses were transformed into a desirability scale. Y_{max} and Y_{min} were considered as the objective function (D) for each response. Finally, each individual desirability function was merged

as a function of geometric mean by extensive grid search and feasibility search over the domain to obtain global desirability value using Design-Expert software. The obtained value of D was close to 1.0000, implying the favorable influence of the selected variables' blend on the response. The level of factors and point prediction model is as shown in fig. 11. Contour plots represent the relationship between a fitted response when considering the study of only two factors in each plot. The darkest zone on the graph shows the highest desirable. The 3-dimensional contour plots showing the relationship between a response value on the Z-axis and two variables on the X-and Y-axes are shown in the fig. 12 [18, 19].

Three executive baths of nanobubbles were generated under ideal circumstances to verify the model's suitability. Fig. 13 depicts the response parameters for the created batches. A close agreement between predicted and experimental values, as shown in fig. 14. The acquired results showed a close resemblance to the anticipated outcomes, proving the viability of the DSD technique in combination with a derringer's desirability strategy for the optimization of sunitinib nanobubbles.

Fig. 11: Optimum level of factors and point prediction
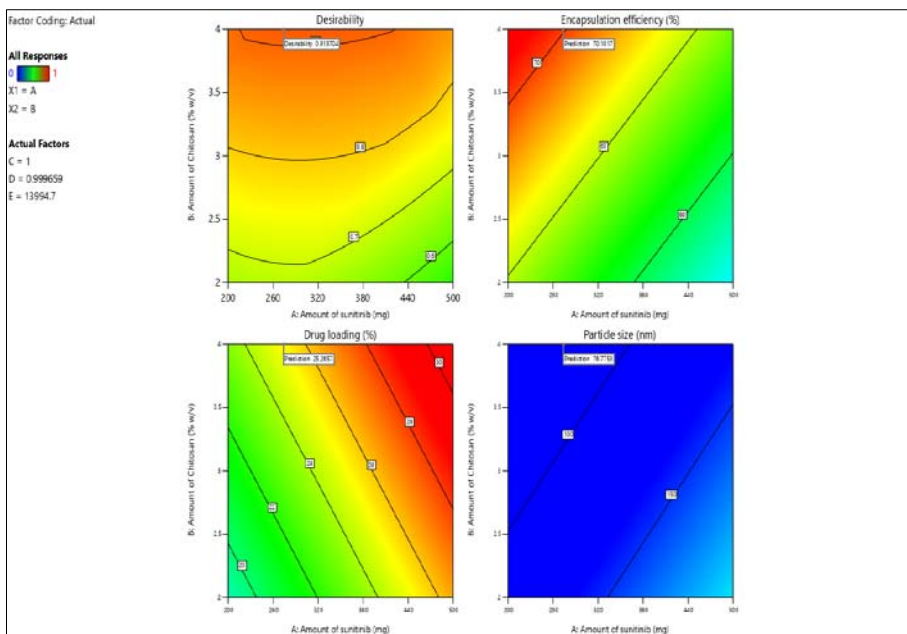
Fig. 12: The 3-dimensional contour plots showing the relationship between a response value on the Z-axis and two variables on the X-and Y-axes

Confirmation Location #1

	Amount of sunitinib	Amount of Chitosan	Amount of Epikuron	Amount of Palmitic acid	Stirring speed
	273.799	3.99972	1	0.999659	13994.7

Response data

Runs: 3

	Encapsulation efficiency	Drug loading	Particle size
	69.56	24.86	80.34
	68.48	25.02	78.56
	68.92	23.88	82.42

Fig. 13: Results of the confirmation experiments

Confirmation

Two-sided   Confidence = 95%

Solution 1 of 100 Response	Predicted Mean	Predicted Median	Observed	Std Dev	n	SE Pred	95% PI low	Data Mean	95% PI high
Encapsulation efficiency	70.1017	70.1017		0.590326	3	0.539587	68.8258	68.9867	71.3776
Drug loading	25.2657	25.2657		0.358274	3	0.32748	24.4914	24.5867	26.0401
Particle size	76.7753	76.7753		4.02493	3	3.67898	68.0759	80.44	85.4748

Fig. 14: Comparison between obtained and predicted results, the polydispersity index, particle size, zeta potential, percent drug filling and encapsulation efficacy values of all the three batches are presented in table 3 [20-22]

Table 3: Physical characteristics of nanobubbles

Blank nanobubbles	Average particle size (nm)	Polydispersity index	Zeta potential (mV)	Encapsulation efficiency (%)	Loading capacity (%)
	79.38±5.63	0.28±0.005	51.82±3.56	--	--
Batch-1	80.34±7.12	0.32±0.005	41.38±2.46	69.56±3.82	24.86±0.94
Batch-2	78.56±3.14	0.26±0.005	38.78±3.12	68.48±4.56	25.02±1.22
Batch-3	82.42±5.62	0.29±0.005	40.12±4.46	68.92±3.12	23.88±1.58

n = 3
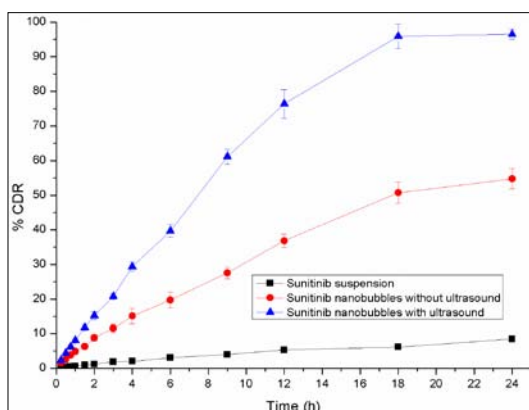
Fig. 15: Drug release patterns *in vitro* with and without ultrasonic support (n = 3)

***In vitro* drug release**

Fig. 15 shows the *in vitro* release profile of sunitinib from nanobubbles in pH 7.4 phosphate barrier solution in the presence or absence of ultrasound treatment to assess the effect of sonication on drug release when compared to the sunitinib solution, the amount of medication released by nanobubbles was much greater. The medicine unconfined with ultrasound help differed significantly from the substance released without ultrasound assistance. Afterwards 6h, the 39.66 % of under

sonication sunitinib was able to be released, whereas only 19.73 percent was able to be released without dispersion. Only 54.76 percent of sunitinib would have been released after 24 h if ultrasonography hadn't been used. On the other hand, ultrasonography allowed for the release of about 96.52 percent of the sunitinib. The findings showed that the cavitation action of ultrasound may facilitate the release of sunitinib from the nanobubbles.

FTIR

FTIR spectra of the sunitinib, chitosan, Epikuron 200, palmitic acid and physical combination showed that substantial distinctive peaks were present, as seen in fig. 16. The main sunitinib characteristic peaks were observed at 3350.46, 3238.59, 2968.55, 2816.16, 2360.95, 2341.66, 1676.20, 1587.47, 1546.96, 1477.52, 1330.93 and 1035.81 cm^{-1}, suggesting that there were no chemical interactions between the medicine and the chosen excipients. With a physical mixture, however, several extra peaks were seen, which could be related to the excipients' functional groups.

DSC

Fig. 17 reports the Thermogravimetric analysis of sunitinib-loaded chitosan nanobubbles performed with differential scanning calorimetry. Sunitinib's DSC curve has an endothermic peak at 248.13 °C, which corresponds to its melting point. The endothermic peak of chitosan's DSC curve is located at 87.82 degrees Celsius. Blank nanobubbles' DSC curve had two endothermic peaks. Water evaporation is associated with the first broad peak, which occurs at around 73.406 °C, whereas the temperature at which the water-embedded chitosan matrix experiences a transition to a glassy state,

is associated with the second broad peak, which occurs in the 90–100 °C range. Chitosan reached a peak temperature of 87.82 degrees Celsius, whereas chitosan nanobubbles showed an endothermic peak temperature of 98.34 degrees Celsius. The structure of the polysaccharide matrix in the nanobubbles has changed, as indicated by the difference in melting temperatures. The elimination of the drug's distinctive endothermic peak indicates that the drug has been completely incorporated into the core structure.
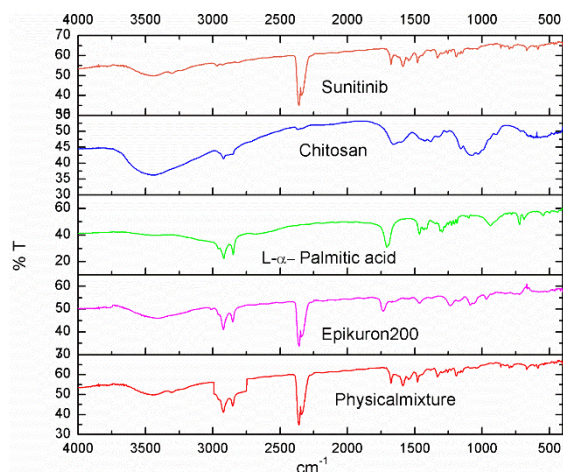
Fig. 16: FTIR spectrum of sunitinib, chitosan, Epikuron 200, palmitic acid and physical mixture
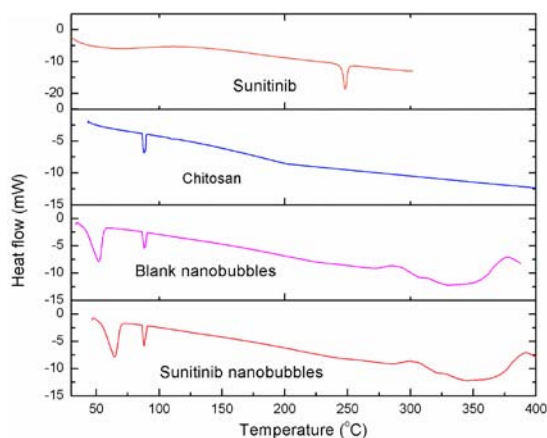
Fig. 17: Chitosan, DSC thermogram of sunitinib, sunitinib loaded nanobubbles and blank nanobubbles

TEM

The morphology of the nanobubbles was observed under the transmission electron microscope. TEM pictures showed the surface morphology and core-shell organisation of nanofroths between 70 and 100 nm in size (fig. 18).
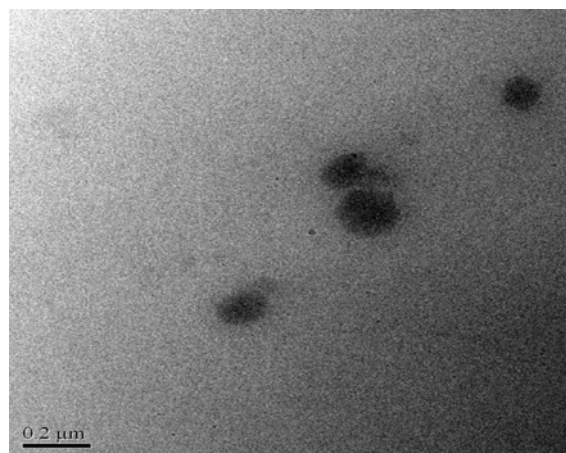
Fig. 18: TEM image of sunitinib nanobubbles

Hemolytic activity

The formulation must not be poisonous in order to be used for parenteral delivery. Therefore, the hemolytic activity of the sunitinib-loaded and blank nanobubbles was assessed in order to assess their safety. Up to the measured concentration of 10 mg/ml, it was found that the aqueous suspensions of chitosan nanobubbles are not hemolytic. With erythrocytes, drug-loaded nanobubbles likewise had a favourable safety profile.

Stability studies

The storage stability of sunitinib nanobubbles was evaluated at different temperatures (4 °C, 25 °C and 40 °C) for 1 mo. The data on drug content, encapsulation efficiency and particle size of sunitinib nanobubbles at 0, 15 and 30 d are shown in table 4. No significant change in drug content was observed at lower temperatures. The encapsulation efficiency hardly changed at 4 °C and 25 °C, indicating that nanobubbles could protect sunitinib from degradation or deterioration at normal temperature. At higher temperature, the encapsulation efficiency is significantly reduced, indicating the disruption of nanobubbles structure at the higher temperature. During the whole stability experiment time, the PDI values of drug-loaded nanobubbles were under 0.3, meaning homogenous size distribution in the formulation.

Table 4: Encapsulation efficiency, particle size, and PDI of sunitinib various temperatures were used to store nanobubbles

Temperature (°C)	Times (days)	Encapsulation efficacy (%)	Particle size (nm)	PDI
4±1 °C	0	68.48±4.56	78.56±3.14	0.26±0.005
	15	68.32±3.46	81.22±4.88	0.27±0.005
	90	68.56±1.92	80.33±3.94	0.24±0.005
	180	67.88±2.48	80.89±6.98	0.26±0.005
25±2 °C	0	68.48±4.56	78.56±3.14	0.26±0.005
	15	67.34±2.32	96.22±4.88	0.29±0.005
	90	66.56±3.24	95.33±3.94	0.30±0.005
	180	66.18±4.26	96.83±5.78	0.32±0.005
40±2 °C	0	68.48±4.56	78.56±3.14	0.26±0.005
	15	64.89±1.98	148.12±1.84	0.31±0.005
	90	61.12±3.06	176.34±2.12	0.38±0.005
	180	56.34±4.82	198.58±4.36	0.43±0.005

n = 3

CONCLUSION

For the administration of the anticancer medication sunitinib, chitosan-shelled and perfluropentane-filled nanobubbles were created in this work. The formulation's constituent parts were enhanced using respect to encapsulation efficiency, percent drug loading and particle size using a definitive screening design. Nanobubbles prepared under optimal conditions exhibited improved encapsulation efficiency and drug loading with unvarying unit magnitude. At all pH levels, the solubility of the sunitinib nanobubbles is much higher than that of the sunitinib solution. Sunitinib nanobubbles have superior dissolving profiles and higher gastrointestinal stability than the suspension, according to an *in vitro* dissolution test, which significantly increases oral bioavailability. Chitosan nanobubbles might be thought of as an intriguing technique in the creation of sunitinib formulations that respond to ultrasound for targeted drug administration.

AUTHORS CONTRIBUTIONS

All the authors have contributed equally.

CONFLICT OF INTERESTS

Declared none

REFERENCES

1. Le Tourneau C, Raymond E, Faivre S. Sunitinib: a novel tyrosine kinase inhibitor. A brief review of its therapeutic potential in the treatment of renal carcinoma and gastrointestinal stromal tumors (GIST). Ther Clin Risk Manag. 2007 Jun;3(2):341-8. doi: 10.2147/tcrm.2007.3.2.341, PMID 18360643.
2. Kassem MG, Motiur Rahman AF, Korashy HM. Sunitinib malate. Profiles Drug Subst Excip Relat Methodol. 2012;37:363-88. doi: 10.1016/B978-0-12-397220-0.00009-X. PMID 22469323.
3. Ramazani F, Hiemstra C, Steendam R, Kazazi Hyseni F, Van Nostrum CF, Storm G. Sunitinib microspheres based on [PDLLA-PEG-PDLLA]-b-PLLA multi-block copolymers for ocular drug delivery. Eur J Pharm Biopharm. 2015 Sep 1;95(B):368-77. doi: 10.1016/j.ejpb.2015.02.011, PMID 25701807.
4. Joseph JJ, Sangeetha D, Gomathi T. Sunitinib loaded chitosan nanoparticles formulation and its evaluation. Int J Biol Macromol. 2016 Jan 1;82:952-8. doi: 10.1016/j.ijbiomac.2015.10.079, PMID 26522243.
5. Nazari Vanani R, Azarpira N, Heli H, Karimian K, Sattarahmady N. A novel self-nano emulsifying formulation for sunitinib: evaluation of anticancer efficacy. Colloids Surf B Biointerfaces. 2017 Dec 1;160:65-72. doi: 10.1016/j.colsurfb.2017.09.008, PMID 28917151.
6. Leggio L, Arrabito G, Ferrara V, Vivarelli S, Paterno G, Marchetti B. Mastering the tools: natural versus artificial vesicles in nanomedicine. Adv Healthc Mater. 2020 Sep;9(18):e2000731. doi: 10.1002/adhm.202000731, PMID 32864899.
7. Bhowmik H, Nagasamy Venkatesh D, Kuila A, Kammari Harish Kumar N. A review. Int J Appl Pharm. 2018;10(4):207-1.
8. Zhang CB, Cao HL, Li Q, Tu J, Guo X, Liu Z. Enhancement effect of ultrasound-induced microbubble cavitation on branched polyethylenimine-mediated VEGF(165) transfection with varied N/P ratio. Ultrasound Med Biol. 2013;39(1):161-71. doi: 10.1016/j.ultrasmedbio.2012.08.025, PMID 23141903.
9. Van den Broek LA, Knoop RJ, Kappen FH, Boeriu CG. Chitosan films and blends for packaging material. Carbohydr Polym. 2015;116:237-42. doi: 10.1016/j.carbpol.2014.07.039, PMID 25458295.
10. Candioti LV, De Zan MM, Camara MS, Goicoechea HC. Experimental design and multiple response optimization. Using the desirability function in analytical methods development. Talanta. 2014 Jun 15;124:123-38. doi: 10.1016/j.talanta.2014.01.034, PMID 24767454.
11. Cavalli R, Bisazza A, Trotta M, Argenziano M, Civra A, Donalisio M. New chitosan nanobubbles for ultrasound-mediated gene delivery: preparation and *in vitro* characterization. Int J Nanomedicine. 2012;7:3309-18. doi: 10.2147/IJN.S30912, PMID 22802689.
12. Babu Dr. Preparation, characterization and evaluation of chitosan nanobubbles for the targeted delivery of ibrutinib. Nat Phenom. 2021.
13. Alshetaili AS, Ansari MJ, Anwer MdK, Ganaie MA, Iqbal M, Alshahrani SM. Enhanced oral bioavailability of ibrutinib encapsulated poly (Lactic-co-glycolic acid) nanoparticles: pharmacokinetic evaluation in rats. Curr Pharm Anal. 2019;15(6):661-8. doi: 10.2174/1573412915666190314124932.
14. Hwang TL, Lin YK, Chi CH, Huang TH, Fang JY. Development and evaluation of perfluorocarbon nanobubbles for apomorphine delivery. J Pharm Sci. 2009;98(10):3735-47. doi: 10.1002/jps.21687, PMID 19156914.
15. Takano S, Kondo H. Quantitative method for determination of hemolytic activity of Clostridium septicum toxin. Japan J Med Sci Biol. 1987;40(2):47-59. doi: 10.7883/yoken1952.40.47, PMID 3430819.
16. Jones B, Nachtsheim CJ. A class of three-level designs for definitive screening in the presence of second-order effects. J Qual Technol. 2011 Jan 1;43(1):1-15. doi: 10.1080/00224065.2011.11917841.
17. Maherani B, Arab Tehrany E, Kheirolomoom A, Reshetov V, Stebe MJ, Linder M. Optimization and characterization of liposome formulation by mixture design. Analyst. 2012;137(3):773-86. doi: 10.1039/c1an15794a, PMID 22158519.
18. Derringer G, Suich R. Simultaneous optimization of several response variables. J Qual Technol. 1980 Oct 1;12(4):214-9. doi: 10.1080/00224065.1980.11980968.
19. Dhiman S, Verma S. Optimization of melt-in-mouth tablets of levocetirizine dihydrochloride using response surface methodology. Int J Pharm Pharm Sci. 2012;4.
20. Hoven VP, Tangpasuthadol V, Angkitpaiboon Y, Vallapa N, Kiatkamjornwong S. Surface-charged chitosan: preparation and protein adsorption. Carbohydr Polym. 2007 Mar 1;68(1):44-53. doi: 10.1016/j.carbpol.2006.07.008.
21. Natarajan, Satheesh, Rajan D, Prabakaran L, Meka Venkata, Perumal Chandran S. Formulation optimization, scale up technique and stability analysis of naproxen loaded lipospheres. Asian J Pharm Clin Res. 2014;7:121-6.
22. Manisha Bhoskar, Priyanka Patil. Development and evaluation of paclitaxel loaded nanoparticles using 2^4factorial design. Int J Curr Pharm Res. 2015;7(2):64-72.